



Article

Geometric Accuracy Analysis of Regional Block Adjustment Using GF-7 Stereo Images without GCPs

Xinming Tang ¹, Xiaoyong Zhu ^{1,*}, Wenmin Hu ² and Jianhang Ding ^{1,3}

¹ The Land Satellite Remote Sensing Application Center, Ministry of Natural Resources, Beijing 100048, China; txm@lasac.cn (X.T.); dingjh@lasac.cn (J.D.)

² The National Joint Engineering Laboratory of Internet Applied Technology of Mines, China University of Mining and Technology, Xuzhou 221116, China; huwm@cumt.edu.cn

³ Faculty of Geomatics, Lanzhou Jiaotong University, Lanzhou 730070, China

* Correspondence: zhuxy@lasac.cn; Tel.: +86-010-68412289

Abstract: As an important means of improving positioning accuracy, block adjustment has been used in the improvement and assessment of accuracy for the Chinese Gaofen-7 (GF-7) satellite. However, there is little research on what factors affect accuracy without ground control points (GCPs). The correlation between accuracy and the images participating in the adjustment is not clear. This paper proposes the correlation coefficients and canonical correlation analysis between five accuracy indicators and three sets of ten adjustment factors, including topographic factors, participating image factors, and tie points (TPs) factors, to quantify the influence of adjustment factors on accuracy. Block adjustment without GCPs for GF-7 stereo imagery is verified in three study areas to evaluate the relationship between accuracy and adjustment factors. The results show that block adjustment without GCPs can improve direct positioning accuracy with an average improvement of 1.27 m in the planar direction and 0.13 m in the elevation direction. Moreover, plane accuracy is more easily affected by three sets of factors, while the influence on elevation accuracy is more balanced. The set of TP factors has the greatest influence on accuracy, and the image overlap is more critical than the image coverage area, number, and time periods. Topographic factors also play an important role, and the influence of the elevation factor with the highest canonical correlation coefficient (-0.71) is more significant than the other two factors, roughness, and slope. The results provide a reference for the improvement of adjustment accuracy without GCPs, the reasonable selection of adjustment images, the optimization of TPs, and the strategy of the partition processing of large-area block adjustment for GF-7 stereo imagery.

Keywords: GF-7; geometric accuracy; block adjustment; correlation coefficients; adjustment factor



Citation: Tang, X.; Zhu, X.; Hu, W.; Ding, J. Geometric Accuracy Analysis of Regional Block Adjustment Using GF-7 Stereo Images without GCPs. *Remote Sens.* **2023**, *15*, 2552. <https://doi.org/10.3390/rs15102552>

Academic Editors: Jiannan Zhao and Ákos Kereszturi

Received: 17 March 2023

Revised: 7 May 2023

Accepted: 7 May 2023

Published: 12 May 2023



Copyright: © 2023 by the authors. Licensee MDPI, Basel, Switzerland. This article is an open access article distributed under the terms and conditions of the Creative Commons Attribution (CC BY) license (<https://creativecommons.org/licenses/by/4.0/>).

1. Introduction

Geometric accuracy has always been the focus of stereo imaging and mapping satellites. As an important means to improve positioning accuracy, block adjustment has been used in many stereo mappings [1–8]. There are many studies regarding the improvement of its method, such as the stable solution in free adjustment without GCPs [9–12], the storing and computing algorithm for large-scale data [13], the determination of appropriate weights for adjustment parameters [12], etc. These studies provide effective methods and thus improve accuracy or efficiency. With the application of more and more high-resolution satellite stereo images, the correlation between accuracy and participating images is also studied for image selection or accuracy improvement. An earlier attempt was made in the application of the SPOT 5 satellite, which used 480 stereo pairs covering the Middle East block to quantify the absolute location performance relative to the block size and determined that the minimum number of stereo pairs necessary for the block to meet the Reference3D[®] specifications was 10 pairs [14]. Liu found that the image matching error of a stereo pair increased linearly with the increase in the convergence angle, and triangulation of fewer

automatically selected images could produce better geopositioning precision than using all the images for LROC NAC images [15]. Tao proposed an optimal selection method that used a rasterized grid voting strategy to extract a minimal subset from extremely redundant satellite images while still maintaining high image quality and sufficient overlap [16].

However, there are many adjustment factors that may affect the results of geometric accuracy, such as the terrain relief in different regions, images involved in the adjustment, external GCPs or reference data, different adjustment methods, etc. Recent studies mainly focus on the improvement of accuracy and methods, but the specific correlation or quantitative relationship between the influencing factors and accuracy is given less attention.

The GF-7 satellite is China's first civil sub-meter high-resolution stereo mapping satellite optical transmission, which was launched on 3 November 2019. It is mainly used for 1:10,000 scale stereo mapping and has been applied in many applications, such as monitoring winter wheat planting areas, height monitoring of typical lake water levels, and 3D building extraction [17–22]. As the main source for topographic data, its geometric accuracy has always been the focus of satellite stereo imagery. Recent research using block adjustment has shown that the root mean square error (RMSE) for elevation accuracy of GF-7 imagery ranges from 3.42 m to 4.68 m, and the RMSE in planar directions is from 3.81 m to 6.39 m without GCPs in different terrain regions [23]. The positioning accuracy will be improved with GCPs or other control information. For example, when four kinds of terrain, including flat land, hills, mountains, and high mountains, are tested with manually laid GCPs, the RMSEs of elevation are 0.96 m, 1.02 m, 1.26 m, and 1.45 m successively, and the plane errors are within 2 m [24]. The 3D laser points acquired by the laser altimeter carried by the GF-7 satellite are used as the GCPs for their high elevation accuracy or combined with stereo imagery in the block adjustment. The elevation errors can be less than 1 m in the joint adjustment, but the improvement of the plane accuracy is limited [23,25,26]. Some scholars use the posteriori compensation model to correct the relative errors in the adjustment, and the horizontal accuracy is obviously improved to less than 1 m [27]. On the other hand, the accuracy comparison of the GF-7 and GFDM satellites of China using digital surface model (DSM) analysis and the image quality for recognition are studied to evaluate the accuracy or quality of GF-7 imagery [28–30]. These studies have verified the accuracy of GF-7 stereo imagery mapping and provide significant support for further application with GF-7 imagery.

Since the swatch width of GF-7 imagery is 20 km, there are a large number of participating images in some block adjustments, but the acquisition time of these images is not consistent. In most applications, GCPs are not always available or cannot be obtained due to some limitations; local block adjustment without GCPs is more common, and its reliability needs to be further evaluated. In addition, the relationship between accuracy and adjustment factors is also necessary to study for further application of images.

In order to reveal the relationship between the accuracy and adjustment factors in the block adjustment of GF-7 stereo imagery without GCPs, this issue proposes the correlation coefficients and canonical correlation analysis between five accuracy indicators and three sets of ten adjustment factors, including topographic factors, participating image factors, and TPs factors, to quantify the influence of adjustment factors on the accuracy. Block adjustment without GCPs for GF-7 stereo imagery is verified in three study areas to evaluate the relationship between accuracy and adjustment factors.

2. Study Areas and Data Sources

The GF-7 satellite operates on a sun-synchronous orbit at a height of 505 km. Two linear-array push-broom panchromatic cameras are equipped on the satellite as the stereo imaging system. The forward camera has a spatial resolution of 0.8 m with a forward tilt of 26° along the direction of satellite flight, while the backward camera has a spatial resolution of 0.65 m with a back tilt of 5° along the direction of satellite flight [31]. Both the front and back cameras have a ground swath of 20 km.

The regional block adjustment of GF-7 stereo imagery without GCPs is tested in three study areas. The first area is the 08HZ region, which is located in Huzhou, in the northern Zhejiang Province of China. The terrain in the 08HZ region is generally inclined from southwest to northeast. The west is mountainous, while the east is plain, and the northwest is alternated with low hills and plains. The elevation range is about 67 m to 1590 m. The second area is the 07MS region, which is located in the Provence-Alpes-Cote d'Azur region of France. The terrain is mainly plain and hilly, with an elevation range of 0~1244 m, and the terrain inclines from east to west. The third area is the 01TJ region, which is located in Tianjin City, China. The region is the transition zone from Yanshan Mountain to the coastal plain, where the general terrain is high in the north and low in the south, descending step by step from the northern mountain to the southeastern coastal plain. The elevation range is about -44 m to 70 m.

Table 1 lists the detailed acquisition times and quantity of GF-7 imagery used in each region, where H1~H5, M1~M7, and T1~T8 represent each acquisition time period of images in this region. They are coded by spatial proximity, not by time proximity. There are 14 image pairs of the GF-7 satellite acquired at five different times in the 08HZ region, 14 image pairs acquired at seven different times in the 07MS region, and 24 image pairs acquired at eight different times in the 01TJ region, respectively. Figure 1 shows the elevations in the three study areas and the coverage image distribution of the GF-7 satellite.

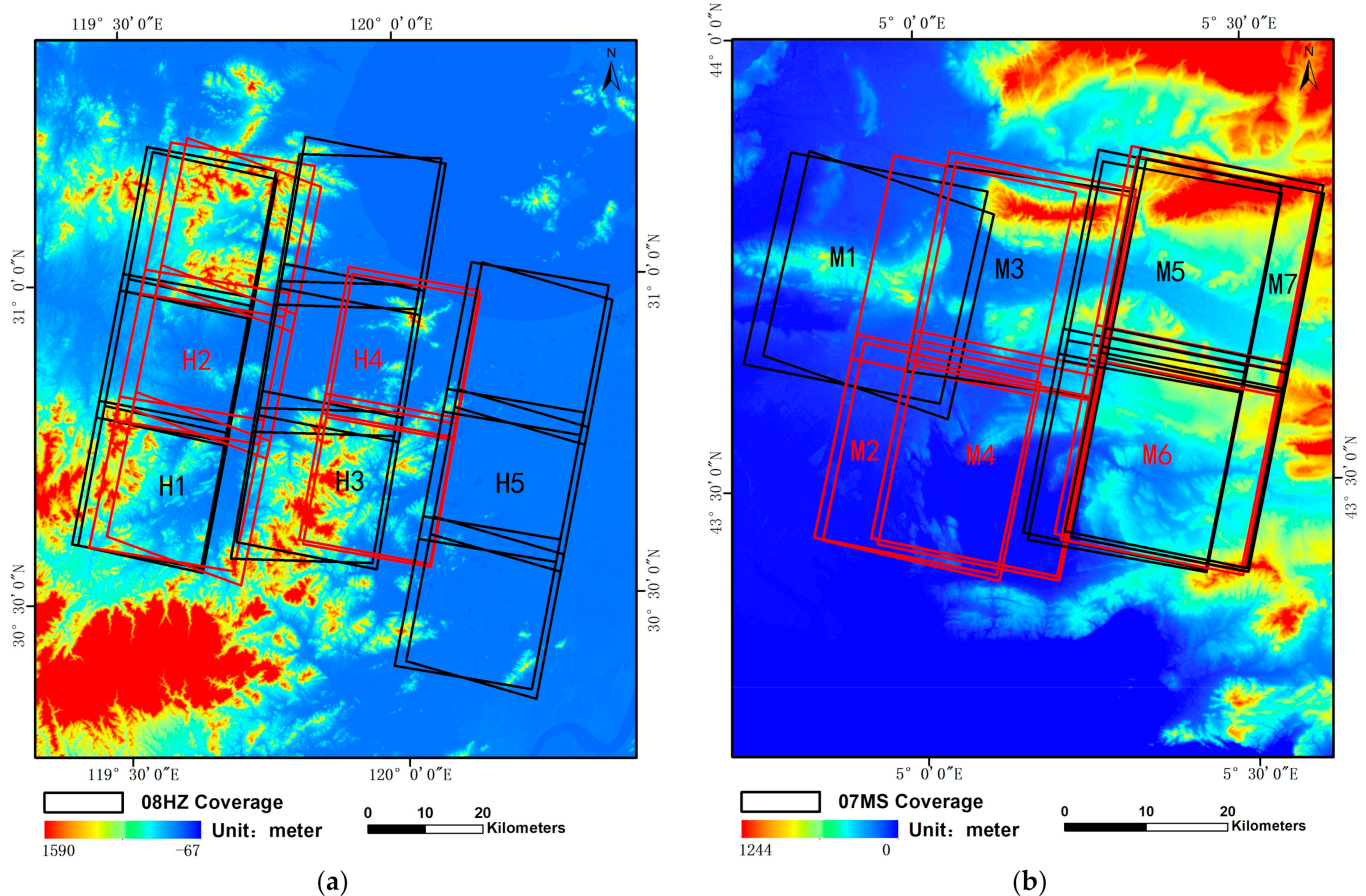


Figure 1. Cont.

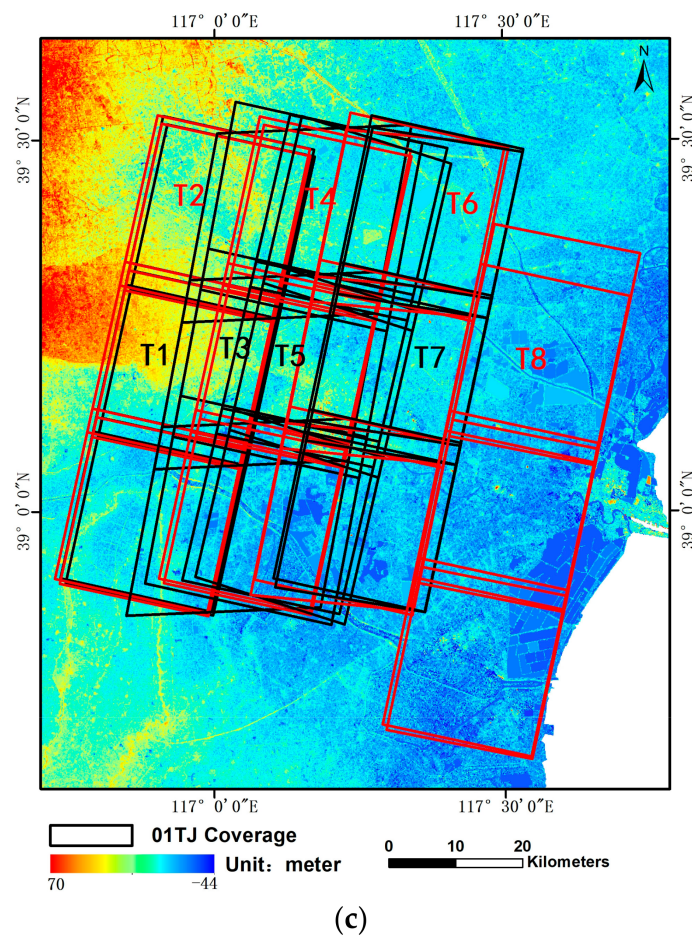


Figure 1. The elevation distribution and image coverage of GF-7 satellite in (a) 08HZ region, (b) 07MS region, and (c) 01TJ region. The labels of H1–H5, M1–M7, and T1–T8 mark the locations of images in each acquisition time period in this region.

Table 1. The acquisition time and quantity of GF-7 imagery used in this study.

08HZ Region		07MS Region		01TJ Region	
Period of Images	Acquisition Time and Quantity of Images	Period of Images	Acquisition Time and Quantity of Images	Period of Images	Acquisition Time and Quantity of Images
H1	26 June 2020 3 pairs (6 scenes)	M1	23 April 2020 1 pair (2 scenes)	T1	24 December 2020 3 pairs (6 scenes)
H2	24 November 2021 3 pairs (6 scenes)	M2	1 July 2020 2 pairs (4 scenes)	T2	19 June 2021 3 pairs (6 scenes)
H3	3 January 2022 3 pairs (6 scenes)	M3	18 May 2020 1 pair (2 scenes)	T3	21 September 2021 3 pairs (6 scenes)
H4	3 September 2020 2 pairs (4 scenes)	M4	3 September 2020 2 pairs (4 scenes)	T4	10 February 2022 3 pairs (6 scenes)
H5	3 May 2020 3 pairs (6 scenes)	M5	28 August 2021 2 pairs (4 scenes)	T5	14 December 2020 3 pairs (6 scenes)
		M6	30 June 2021 2 pairs (4 scenes)	T6	22 May 2020 3 pairs (6 scenes)
		M7	2 May 2021 2 pairs (4 scenes)	T7	5 November 2020 3 pairs (6 scenes)
				T8	1 May 2021 3 pairs (6 scenes)

3. Methods

The correlation between the accuracy indicators and related factors for regional block adjustment is analyzed in this paper. A method using correlation coefficients (CCs) and a canonical correlation model (CCM) for GF-7 stereo images is proposed to construct the relationship between the accuracy indicators and related adjustment factors, and then the assessment of the accuracies of GF-7 images without GCPs is obtained from the revealed relationship. The specific method is shown in Figure 2. First, block adjustments are carried out for images acquired at different periods in the region, and the number of images participating in the adjustment is gradually increased. TPs are generated according to the images participating in adjustment using SIFT in each adjustment combination; then, the error equation of the block using the rational function model (RFM) will be constructed, and the parameters obtained by the iteration will be used to calculate the three-dimensional ground coordinates in the object space using the forward intersection. Second, accuracy indicators in image space and object space are validated using TPs between the images in the study area and the reference images and virtual GCPs. Then, the set of accuracy variables and the factors affecting the image adjustment accuracy, including regional topographic factors, image factors, and TPs factors, are selected. Finally, the accuracy correlation coefficient and canonical correlation model between the accuracy indicators and three kinds of adjustment factors are constructed.

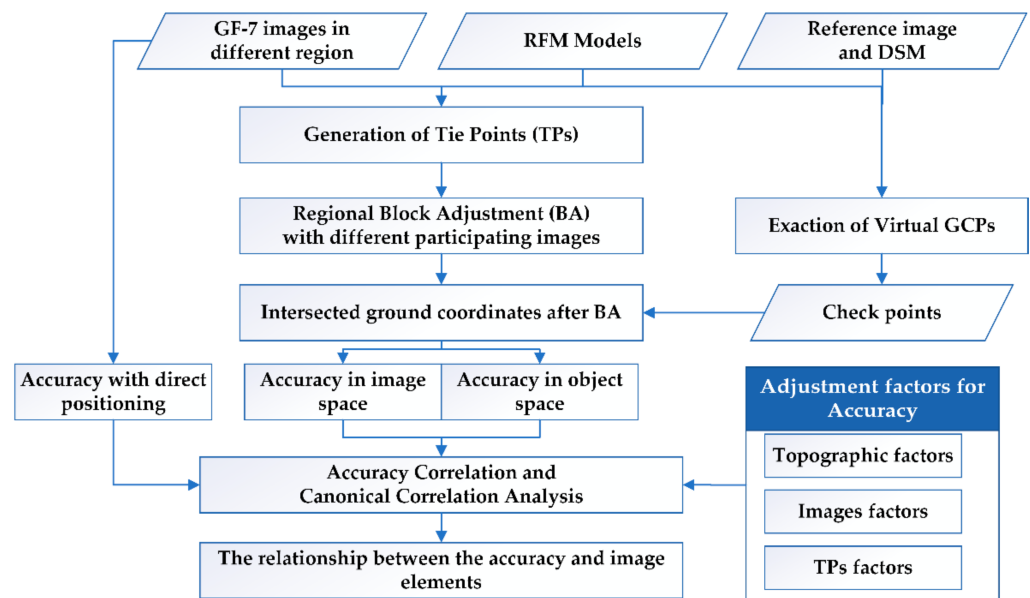


Figure 2. Accuracy assessment using Correlation Coefficients and Canonical Correlation Analysis for GF-7 regional images.

3.1. Regional Block Adjustments of Stereo Images Using RFM

As a more general expression, RFM is an accurate fitting of the rigorous geometric imaging model and is widely used in the geometric adjustment of satellite remote sensing imagery. In the RFM, the relationship between the image pixel coordinates and the corresponding ground three-dimensional coordinates can be described as the ratio polynomials as follows:

$$l = \frac{P_1(lon, lat, h)}{P_2(lon, lat, h)}, s = \frac{P_3(lon, lat, h)}{P_4(lon, lat, h)} \quad (1)$$

where (l, s) are the image pixel coordinates and (lon, lat, h) are their corresponding normalized ground geodetic coordinates, P_1, P_2, P_3, P_4 are the rational polynomial coefficients (RPC) of the RFM. In general, the distortion due to the optical projections is expressed as first-order polynomials; the imaging deformation caused by atmospheric refraction, Earth curvature, lens distortion, and satellite GPS/IMU inherent errors can be approximated by

the quadratic polynomial; and the higher-order unknown distortion is described by the third-order. Therefore, the powers of each coordinate component in the polynomial are no more than 3. Since the geometric imaging model of GF-7 images has been well calibrated, an affine transformation of the image refinement model is adopted to compensate for the errors of RFM. The error equation is described in

$$\begin{cases} \Delta l = a_0 + a_1 \cdot s + a_2 \cdot l \\ \Delta s = b_0 + b_1 \cdot s + b_2 \cdot l \end{cases} \quad (2)$$

where $(\Delta l, \Delta s)$ are the corrections for the image coordinates, (l, s) are the observations of the imagery coordinates, and $(a_0, a_1, a_2, b_0, b_1, b_2)$ are the coefficients of the affine model. Then, the block adjustment model can be expressed as follows:

$$\begin{cases} F_l = \frac{P_1(lon,lat,h)}{P_2(lon,lat,h)} - l - \Delta l \\ F_s = \frac{P_3(lon,lat,h)}{P_4(lon,lat,h)} - s - \Delta s \end{cases} \quad (3)$$

Taking the affine coefficients of the RFM and the corresponding ground coordinates for the TPs as unknowns, the error equation for each tie point in the block adjustments can be constructed as follows:

$$V = Ax + Bt - LP \quad (4)$$

where V are the residual vectors of the TPs; x is the correction vector of the affine transformation parameters; t is the correction vector of the ground coordinates corresponding to the TPs; A and B are the partial derivative coefficient matrices corresponding to x and t , respectively; L are the constant vectors calculated from the current block adjustment coefficients; and P are the weight matrices determined by the measurement precision of image coordinates for the TPs. The values of x and t are obtained iteratively, and the RPC is refined and updated accordingly during the iteration.

3.2. Validation of Accuracy

Virtual GCPs extracted from the high-resolution reference data are introduced to evaluate the geometric accuracy of GF-7 images after block adjustments. The reference data are DSM obtained from 20 cm aerial imagery after manual editing, and the horizontal and vertical accuracies are both better than 0.4 m. A phase correlation matching algorithm is adopted to achieve registration between the images in the study area and the reference images. Then, the high-precision matching points are obtained as the virtual GCPs, and the corresponding reference elevations are extracted.

Assuming there are m virtual GCPs extracted, $[X_{Vi}, Y_{Vi}, H_{Vi}]$ are the i th 3D ground coordinates of one virtual GCP in the Earth-centered fixed coordinate system WGS-84 UTM, and $[X'_{Vi}, Y'_{Vi}, H'_{Vi}]$ are the corresponding 3D ground coordinates from the benchmark DSM in WGS-84 UTM; then, the elevation deviation at this virtual GCP is

$$V_{Hi} = H_{Vi} - H'_{Vi}, \quad i = 1, \dots, m \quad (5)$$

The elevation deviations of all virtual GCPs are calculated according to Formula (5), and then the RMSE of the elevation deviation is

$$\delta_H = \sqrt{\frac{\sum_{i=1}^m (V_{Hi} - \overline{V_H})^2}{m-1}} \quad (6)$$

where $\overline{V_H} = \frac{1}{m} \sum_{i=1}^m V_{Hi}$, which is the average of the elevation deviations of all GCPs. Similarly, the horizontal deviations can be expressed as

$$\begin{cases} V_{Xi} = X_{Vi} - X'_{Vi} \\ V_{Yi} = Y_{Vi} - Y'_{Vi} \end{cases}, \quad i = 1, \dots, m \quad (7)$$

and the RMSEs of the horizontal deviations are

$$\begin{cases} \delta_X = \sqrt{\frac{\sum_{i=1}^m (V_{Xi} - \bar{V}_X)^2}{m-1}} \\ \delta_Y = \sqrt{\frac{\sum_{i=1}^m (V_{Yi} - \bar{V}_Y)^2}{m-1}} \end{cases} \quad (8)$$

where $\bar{V}_X = \frac{1}{m} \sum_{i=1}^m V_{Xi}$, $\bar{V}_Y = \frac{1}{m} \sum_{i=1}^m V_{Yi}$, which represent the average deviations in the horizontal X, Y directions, respectively. These three RMSE variables are taken as accuracy indicators in object space.

In the image space, the residuals of TPs are used to evaluate the accuracy. The object coordinates calculated by the front intersection of TPs are back projected to the image space using the refined RPC to obtain the corresponding image coordinates (l', s') . The image coordinates of TPs obtained by matching are (l, s) , and the image residual of this TP is

$$\begin{cases} V_l = l - l' \\ V_s = s - s' \end{cases} \quad (9)$$

Similarly, the RMSEs of all TPs' image residuals can be obtained.

$$\begin{cases} \delta_l = \sqrt{\frac{\sum_{i=1}^{m_t} (V_{l,i} - \bar{V}_l)^2}{m_t-1}} \\ \delta_s = \sqrt{\frac{\sum_{i=1}^{m_t} (V_{s,i} - \bar{V}_s)^2}{m_t-1}} \end{cases} \quad (10)$$

where m_t is the number of TPs, $\bar{V}_l = \frac{1}{m_t} \sum_{i=1}^{m_t} V_{l,i}$, $\bar{V}_s = \frac{1}{m_t} \sum_{i=1}^{m_t} V_{s,i}$, which represent the average residuals in the image line and sample directions, respectively. The two RMSE variables are taken as accuracy indicators in image space.

3.3. Accuracy Correlation Coefficient and Canonical Correlation Analysis

In order to verify the influence characteristics of the factors involved in the block adjustment on the accuracy, the correlation coefficient between each factor and the corresponding accuracy is used to describe the relationship between the two. Suppose that one factor variable affecting the adjustment accuracy is X_a and the resulting adjustment accuracy is Y_b , then the correlation coefficient between the two is

$$r(X_a, Y_b) = \frac{Cov(X_a, Y_b)}{\sigma(X_a)\sigma(Y_b)} = \frac{\sum_1^n (X_{a,i} - \bar{X}_a)(Y_{b,i} - \bar{Y}_b)}{\sqrt{\sum_1^n (X_{a,i} - \bar{X}_a)^2 \sum_1^n (Y_{b,i} - \bar{Y}_b)^2}} \quad (11)$$

where $\bar{X}_a = \frac{\sum_1^n (X_{a,i})}{n}$, $\bar{Y}_b = \frac{\sum_1^n (Y_{b,i})}{n}$, n represents the number of experimental results using block adjustments. Values of the correlation coefficient can range from -1 to 1 . A value of -1 indicates a perfect negative correlation, while a value of 1 indicates a perfect positive correlation. A value of 0 indicates no correlation between the columns.

The correlation coefficient describes the linear relationship between each single accuracy variable and each adjustment factor. On this basis, the method of canonical correlation analysis is introduced here to obtain the correlation between the adjustment factors group and the accuracy group [32]. Assuming that a set of adjustment factors is $\mathbf{X} = [x_1, x_2, \dots, x_p]^T$, x_i ($i = 1, \dots, p$) represents each adjustment factor that affects accuracy, p is the number of the adjustment factors; the set of accuracy indicators is $\mathbf{Y} = [y_1, y_2, \dots, y_q]^T$, y_j ($j = 1, \dots, q$) represents each accuracy variable, and q is the number of accuracy indicators. Each set of variables can be linearly reassembled into new groups of canonical correlation variables as

$$\begin{cases} \mathbf{u} = \boldsymbol{\alpha}^T \mathbf{X} = \sum_{i=1}^p \alpha_i x_i \\ \mathbf{v} = \boldsymbol{\beta}^T \mathbf{Y} = \sum_{j=1}^q \beta_j y_j \end{cases} \quad (12)$$

where $\boldsymbol{\alpha}^T$ and $\boldsymbol{\beta}^T$ are the matrices of canonical coefficients. \mathbf{u} is the vector of canonical scores for the \mathbf{X} variables, and \mathbf{v} is the vector of canonical scores for the \mathbf{Y} variables. The original two sets of variables can be represented as k sets of canonical correlation variables $(\mathbf{u}_k, \mathbf{v}_k)$, $k \leq \min(p, q)$. In addition, the coefficients maximize the Pearson correlation coefficient $r(\mathbf{u}, \mathbf{v})$, subject to being uncorrelated to all previous canonical scores and scaled, so that \mathbf{u} and \mathbf{v} have zero mean and unit variance. The related relationship between the adjustment factors and the variables of accuracies can be converted to the solution of $r(\mathbf{u}, \mathbf{v})$ maximum.

$$\begin{aligned} \max r(\mathbf{u}, \mathbf{v}) &= \max \frac{\text{Cov}(\mathbf{u}, \mathbf{v})}{\sigma(\mathbf{u})\sigma(\mathbf{v})} \\ \text{s.t. } \boldsymbol{\alpha}^T D(\mathbf{X})\boldsymbol{\alpha} &= 1; \boldsymbol{\beta}^T D(\mathbf{Y})\boldsymbol{\beta} = 1 \end{aligned} \quad (13)$$

where $D(\mathbf{X})$ and $D(\mathbf{Y})$ are the variances of the adjustment factors and the variance of the accuracy variables, respectively. $\text{Cov}(\mathbf{u}, \mathbf{v})$ is the covariance of (\mathbf{u}, \mathbf{v}) , $\sigma(\mathbf{u})$ and $\sigma(\mathbf{v})$ are the standard deviations of $\sigma(\mathbf{u})$ and $\sigma(\mathbf{v})$, respectively. Then the canonical correlation between \mathbf{u} and \mathbf{v} can be used to analyze the correlation between the original two groups of variables. Then, the correlation coefficient between each original adjustment factor x_i and each canonical correlation variable u_j can be acquired by

$$r(x_i, u_j) = \sum_{k=1}^p \alpha_{kj} \text{Cov}(x_i, x_k) / \sqrt{D(x_i)}, j = 1, \dots, f \quad (14)$$

where f is the number of selected canonical correlation variables.

3.4. Selection of Block Adjustment Factors

The accuracy indexes of stereo surveying and mapping satellite imagery mainly include image square accuracy and object square accuracy. Therefore, the set of accuracy indicators \mathbf{Y} consists of five RMSE variables in Section 3.2: δ_l and δ_s , which are the RMSE of V_l and the RMSE of V_s in image space; δ_X , δ_Y , and δ_H , which are three RMSEs of residuals in object space.

The important factors affecting image adjustment accuracy should be the adjustment method and image data source. In addition, other external factors also have an important impact on the accuracy of the results. Under the premise of the same adjustment method (RFM) and the same data source (GF-7), three types of ten factors affecting adjustment are selected as the adjustment factors in this paper. The first type is a set of regional topographic factors for the ground covered by the imagery, including the average elevation x_1 , the average slope x_2 , and the average roughness x_3 of the terrain in the region. The calculation of these topographic parameters is based on the DEM data ASTER GDEM2, which has a resolution of 30 m and is available as open source [33]. The average elevation can be acquired by

$$x_1 = \sum_{i=1}^{n_a} (h_i) / n_a \quad (15)$$

where n_a is the number of grids in the region, and the elevation of each grid is h_i , $i = 1, \dots, n_a$. The slope describes the rate of elevation change from each grid to its neighbors. The algorithm used to calculate the slope is

$$g_i = 180 * \frac{\text{atan}\left(\sqrt{\left(\frac{\Delta h_i}{\Delta x_i}\right)^2 + \left(\frac{\Delta h_i}{\Delta y_i}\right)^2}\right)}{\pi}, i = 1, \dots, n_a \quad (16)$$

where Δh_i represents the elevation rise for each grid relative to its neighbors, Δx_i and Δy_i are the distance rises in the two horizontal directions from the center grid. Then the average slope can be acquired by

$$x_2 = \sum_{i=1}^{n_a} (g_i) / n_a \quad (17)$$

Here, a 3×3 neighborhood window is used. Similarly, the roughness $r_i = h_{i_max} - h_{i_min}$ is the difference between the maximum and minimum elevations in the window. Then the average roughness can be acquired by

$$x_3 = \sum_{i=1}^{n_a} (r_i) / n_a \quad (18)$$

The second type is a set of participating image factors, including the area of the region images covered (x_4), the number of images (x_5), the number of periods of the participated image (x_6), and the degree of overlap between images (x_7), which is the ratio of the overlapping area between image pairs to the area of the region images covered. It can be calculated as $x_7 = s_o / x_4$, where s_o is the overlapping area between image pairs.

The third type is a set of image TPs factors, which includes the number (x_8) and density (x_9) of TPs participating in adjustment and the nearest neighbor coefficient (x_{10}) of TPs. Where, $x_9 = x_8 / x_4$, which represents the number of TPs per square kilometer. The nearest neighbor coefficient (x_{10}) is calculated by the ratio of the observed average nearest neighbor distance (\bar{d}_{min}) to the expected mean distance ($E(d_{min})$) for TPs given in a random pattern. The specific formula is as follows:

$$x_{10} = \frac{\bar{d}_{min}}{E(d_{min})} = \frac{\sum d_{min} / x_8}{1/2\sqrt{x_9/x_4}} = 2\sqrt{x_9} \sum d_{min} / x_8 \quad (19)$$

where d_{min} equals the distance between each TP and its nearest neighboring TP. It should be noted that the nearest neighbor coefficient is a measure to describe the degree of spatial aggregation for TPs. The larger the value, the more uniform the distribution of TPs.

4. Results

In order to verify and analyze the influence of different factors on accuracy, the adjustment experiments are carried out in three study areas. The accuracy results of regional block adjustments are first generated from different combinations, and they are compared with the results derived from direct positioning with the original RPC. Then, correlation coefficients and a canonical correlation model are calculated and constructed between the accuracy indicators and adjustment factors; the relationship results are listed in the following sections.

4.1. Accuracy of Regional Block Adjustments

According to the method described in Sections 3.1 and 3.2, the block adjustments are carried out based on the TPs generated on each image; 47,649 pairs of TPs are identified from the overlap areas in all three regions. Then, the geometric accuracies of regional images are checked using virtual GCPs generated from high-precision aerial imagery and DSM as the reference data. The results of direct positioning with the original RPC are derived from the satellite auxiliary data and calibration results, which are refined on the ground using the same on-orbit calibration parameters [23,28].

Table 2 shows the comparison between the accuracy from direct positioning with the original RPC and that from block adjustment in three regions. In the 08HZ region, the average RMSE values from direct positioning are 2.51 m, 2.84 m, and 2.89 m for X, Y, and elevation errors, respectively. The average residuals after block adjustment for each single period are 1.35 m, 2.99 m, and 3.15 m for X, Y, and elevation directions, respectively. The main improvement is in the X direction, while the accuracy in the other two directions is slightly worse. After block adjustment with all images in the region, the RMSEs of the overall residuals decrease to 0.99 m, 1.67 m, and 2.66 m, respectively. In the 07MS region, the average RMSE values from direct positioning are 2.85 m, 3.36 m, and 3.66 m for X, Y, and elevation errors, respectively. Similarly, the average accuracy in each single period

after block adjustment is also slightly worse for the Y and elevation directions but only slightly improved in the X direction. Additionally, the RMSEs of the overall residuals are respectively down to 2.83 m, 0.91 m, and 2.78 m after block adjustment with all images in the 07MS region. In the 01TJ region, the average RMSE values of X and Y plane errors from direct positioning decrease from 2.32 m and 3.43 m to 0.70 m and 2.60 m, respectively, while the elevation error increases from 3.39 m to 4.11 m after block adjustment. More specific results have been listed in Tables A3–A5 in the appendix for each single image pair.

Table 2. The accuracy statistics before and after block adjustment in 08HZ, 07MS, and 01TJ regions.

Region	Average Residuals with Direct Stereo Positioning before Block Adjustment (Meter)			Average Residuals after Block Adjustment for Each Single Period (Meter)			Residuals after Block Adjustment with All Images in this Region (Meter)		
	X-RMSE	Y-RMSE	H-RMSE	X-RMSE	Y-RMSE	H-RMSE	X-RMSE	Y-RMSE	H-RMSE
08HZ	2.51	2.84	2.89	1.35	2.99	3.15	0.99	1.67	2.66
07MS	2.85	3.36	3.66	2.40	3.44	3.16	2.83	0.91	2.78
01TJ	2.32	3.43	3.39	2.05	3.33	3.77	0.70	2.60	4.11
Average	2.56	3.21	3.31	1.93	3.25	3.36	1.51	1.73	3.18

Figure 3 shows the accuracy of direct positioning and block adjustment in each single period. From the results, the fluctuation of direct positioning accuracy is from 0.54 m~6.78 m in the planar direction and from 0.82 m~8.51 m in the elevation direction. From April 2020 to February 2022, the residuals with direct stereo positioning change relatively little, with average RMSE values of 2.56 m, 3.21 m, and 3.31 m in the X, Y, and elevation directions, respectively. The positioning accuracy does not deteriorate with time for GF-7 satellite imagery. According to the results in the three regions, the adjustment with images in each single period mainly improved the accuracy in the plane direction, mainly in the X direction, with the average residuals decreasing by 0.63 m, while the accuracy in the other two directions was slightly worse or little improved, with the average residuals increasing by 0.04 m and 0.05 m. However, the regional block adjustment with all images participating in this region has an average improvement of 1.27 m on the plane direction and an improvement range of 0.02 m to 2.45 m, while the average improvement on the elevation direction is only 0.13 m.

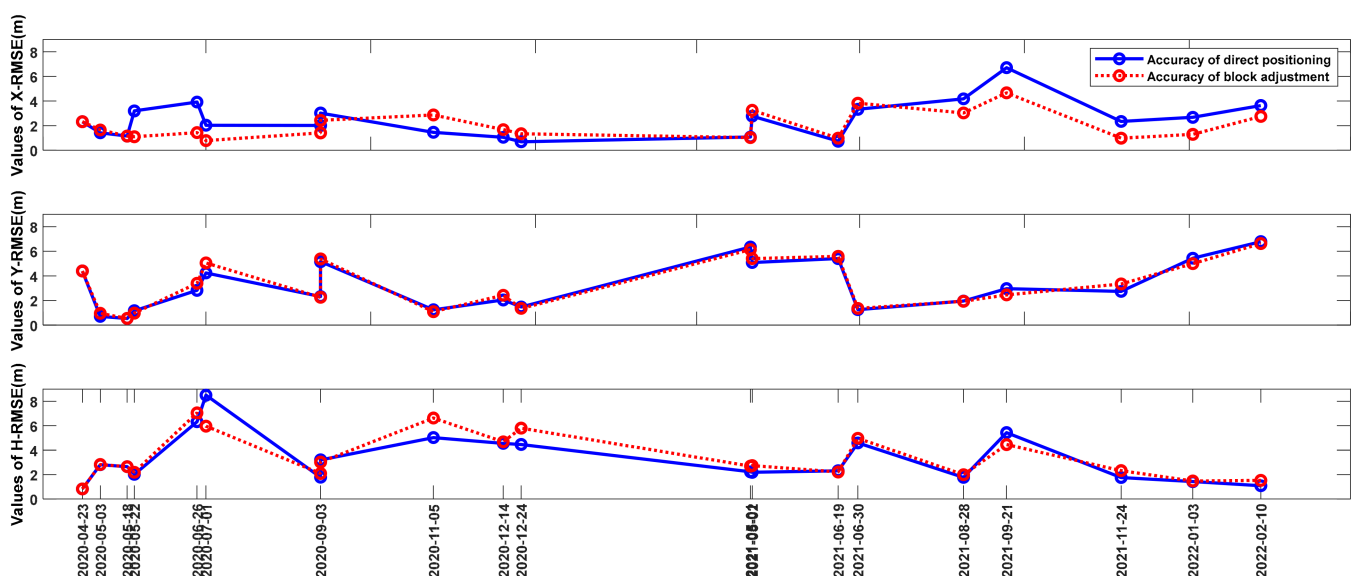


Figure 3. The accuracy of direct positioning and block adjustment in each single period.

Tables 3–5 list the accuracy statistics of different combinations according to spatial proximity using block adjustment in the 08HZ, 07MS, and 01TJ regions, respectively. With

the continuous increase in time periods, the number of images participating in adjustment also increases, and the adjustment results are recorded successively.

Table 3. The accuracy statistics of different combinations using block adjustment in 08HZ region.

Periods of Participated Images	Number of Images Pairs	Residuals in Image Space (Pixel)		Residuals in Object Space (Meter)		
		<i>s</i> -RMSE	<i>l</i> -RMSE	<i>X</i> -RMSE	<i>Y</i> -RMSE	<i>H</i> -RMSE
5 (H1 H2 H3 H4 H5)	14	1.09	2.90	0.99	1.67	2.66
4 (H1 H2 H3 H4)	11	1.22	2.60	0.75	1.55	3.57
3 (H1 H2 H3)	9	1.81	3.15	0.95	2.27	2.29
2 (H1 H2)	6	1.19	1.94	1.21	1.06	2.60
1 (H1)	3	1.42	7.14	1.43	3.40	7.05

Table 4. The accuracy statistics of different combinations using block adjustment in 07MS region.

Periods of Participated Images	Number of Images Pairs	Residuals in Image Space (Pixel)		Residuals in Object Space (Meter)		
		<i>s</i> -RMSE	<i>l</i> -RMSE	<i>X</i> -RMSE	<i>Y</i> -RMSE	<i>H</i> -RMSE
7 (M1M2M3M4M5M6M7)	14	4.12	2.24	2.83	0.91	2.78
6 (M1M2M3M4M5M6)	12	3.68	3.05	2.80	1.48	2.38
5 (M1M2M3M4M5)	8	3.41	3.03	2.60	1.30	2.74
4 (M1M2M3M4)	6	2.65	3.68	2.21	1.76	2.68
3 (M1M2M3)	4	3.73	2.37	2.18	1.91	3.46
2 (M1M2)	3	2.79	2.55	1.74	2.26	2.80
1 (M1)	1	4.80	6.35	4.22	3.87	1.75

Table 5. The accuracy statistics of different combinations using block adjustment in 01TJ region.

Periods of Participated Images	Number of Images Pairs	Residuals in Image Space (Pixel)		Residuals in Object Space (Meter)		
		<i>s</i> -RMSE	<i>l</i> -RMSE	<i>X</i> -RMSE	<i>Y</i> -RMSE	<i>H</i> -RMSE
8 (T1T2T3T4T5T6T7T8)	24	1.37	3.83	0.70	2.60	4.11
7 (T1T2T3T4T5T6T7)	21	1.39	3.48	0.72	2.63	2.92
6 (T1T2T3T4T5T6)	18	1.71	3.71	0.74	3.01	2.61
5 (T1T2T3T4T5)	15	1.94	4.13	0.82	3.36	2.98
4 (T1T2T3T4)	12	3.01	4.94	1.39	4.07	1.75
3 (T1T2T3)	9	1.98	4.03	0.82	3.28	2.39
2 (T1T2)	6	1.21	4.10	0.67	3.27	3.57
1 (T1)	3	1.74	2.99	1.15	1.41	5.88

Although there are small fluctuations, the residuals in image space and object space gradually decrease with the increase in the number of participating images. For example, the *s*-RMSE and *l*-RMSE in the H1 period are 1.42 and 7.14 pixels, respectively, and they are reduced to 1.09 and 2.90 pixels after the images from the H1~H5 five periods participated in the block adjustment. Similarly, the residuals in object space also decrease from 1.43 (*X*-RMSE), 3.40 (*Y*-RMSE), and 7.05 (*H*-RMSE) meters to 0.99 (*X*-RMSE), 1.67 (*Y*-RMSE), and 2.66 (*H*-RMSE) meters. The results in the 07MS region are similar to those in the 08HZ region, with RMSE values in the *s*, *l*, *X*, and *Y* directions decreasing by 0.56 pixels, 4.11 pixels, 1.39 m, and 2.96 m, respectively. While the RMSE value in the *H* direction increases by 1.03 m. The 01TJ region is slightly different from the previous two regions in that there are some fluctuations for both planer and elevation errors. As shown in Table 5, the RMSE values in the *s*, *X*, and *H* directions decrease by 0.37 pixels, 0.45 m, and 1.77 m, respectively, but the RMSE values in the *l* and *Y* directions increase by 0.84 pixels and 1.19 m, respectively.

4.2. Correlation Coefficients between the Accuracy Indicators and Adjustment Factors

Ten adjustment factors from three types of region topography, participating images, and image TPs are selected closely related to accuracy. Figure 4 shows the distribution of correlation coefficients between five accuracy indicators and ten adjustment factors.

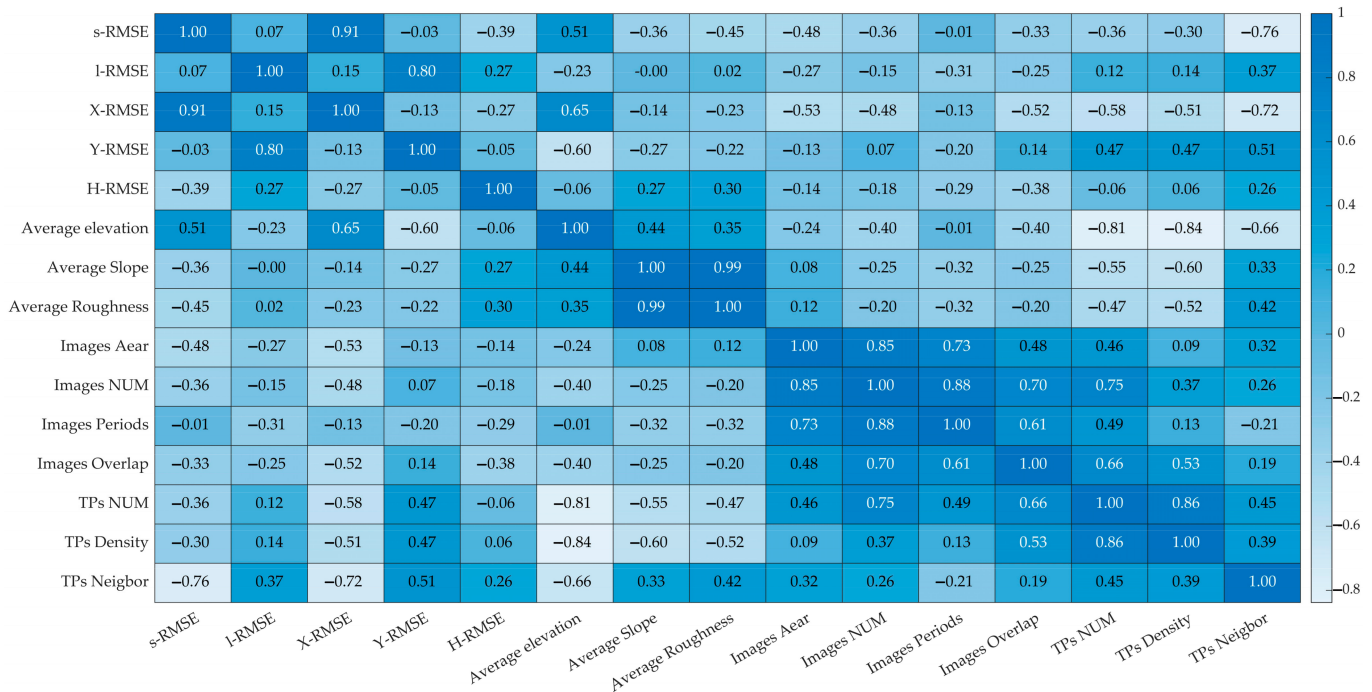


Figure 4. Correlation coefficients between the accuracy indicators and the block adjustment factors.

(1) The relation between accuracy indicators in image space and adjustment factors from the correlation coefficients.

The main three factors affecting the accuracy in image space in the *s* direction are the nearest neighbor coefficient of TPs (CC is -0.76), the average elevation (CC is 0.51), and the area of the region images covered (CC is -0.48). While the main factors affecting the accuracy in the *l* direction are the nearest neighbor coefficient of TPs (CC is -0.37) and the set of participating image factors, in which the effects from the image periods (CC is -0.31), the area of the region images covered (CC is -0.27), and the image overlap (CC is -0.25) are very close.

When the coefficients in both directions are considered together, the factors affecting the accuracy of the image space are the set of image TPs factors, the set of participating image factors, and the set of regional topographic factors in order of importance (with the influence degree from the highest to the lowest), respectively. The three largest factors are the nearest neighbor coefficient of TPs (1.03), image area (0.75), and average terrain elevation (0.74) from the three sets. Moreover, the number of images and the degree of overlap in the set of participating images have higher CC values (0.61 and 0.58). That means the set of participating image factors plays a more important role in the accuracy of image space than regional topographic factors.

In addition, the accuracy correlation between *s* and *l* directions is not obvious (CC is 0.07), but it is strongly correlated with the corresponding accuracy of X and Y directions in object space. The CCs are 0.91 and 0.80 , respectively.

(2) The relation between accuracy indicators in object space and adjustment factors from the correlation coefficients.

The main factors affecting the accuracy of X direction in object space are the nearest neighbor coefficient, the number and density of TPs (CCs are -0.72 , -0.58 , -0.51 , respectively), and the average elevation (CC is 0.65) from a set of regional topographic factors.

The degree of overlap (CC is -0.52), the area (CC is -0.53), and the number (CC is -0.48) of images from participating images also have a great influence on the accuracy. In contrast to the X direction, the set of participating image factors has a lower impact on the accuracy of the Y direction. The main factors affecting the accuracy in object space in the Y direction are the average elevation (CC is -0.60), the nearest neighbor coefficient, and the number and density of TPs (CCs are 0.51, 0.47, and 0.47, respectively). It can be seen that the set of TP factors and the average elevation from regional topographic factors are the main factors with great influence on the plane's accuracy.

However, the CCs for *H*-RMSE from three-factor sets are all small and close, such as the roughness (CC is 0.30) and the slope (CC is 0.27) factors, the degree of overlap (CC is -0.38) and image periods (CC is -0.29) factors, and the nearest neighbor coefficient of TPs factors (CC is 0.26). That means the impacts from the three sets of factors are more balanced on elevation accuracy.

Similarly, when the coefficients in three directions are considered together, the factors affecting the accuracy in object space from the largest to the smallest are the set of image TPs factors, the set of regional topographic factors, and the set of participating image factors. The main five largest factors are the nearest neighbor coefficient of TPs (1.59), average terrain elevation (1.31), number of TPs (1.11), density of TPs (1.04), and the degree of overlap between images (1.04).

It can be seen that the accuracy indicators in object space are strongly correlated with three sets of factors. Moreover, the TPs factors have a greater influence on the three directions, especially on the X and Y directions. The influence of average elevation from topographic factors is also more obvious in the X and Y directions, while in terms of elevation accuracy, slope, and roughness are more influential. In the set of participating image factors, the overlap of the image plays a greater role than other factors in accuracy.

4.3. Relationship from Canonical Correlation Analysis

Twenty sets of adjustment factors (*X*) and twenty sets of accuracy indicators (*Y*) are derived from the results of twenty adjustment experiments and the corresponding attribute information in the three study regions. The specific values of the datasets are listed in Tables A1 and A2 in the Appendix A. The canonical correlation coefficients between the set of adjustment factors and the set of accuracy indicators are calculated using the method in Section 3.3, and then the structures of the canonical correlation model are constructed to obtain the mutual correlation between the two sets.

Table 6 lists all five canonical correlation coefficients of $r(u, v)$ and the statistics of the hypothesis test using the likelihood ratio method, which is used to check whether the difference between the approximate chi-squared statistic for canonical correlation coefficients and the critical value is significant. The results show that the first three canonical correlation coefficients are all high, especially the coefficient for the first canonical correlation variables (u_1, v_1) is 0.99, which is very close to 1, indicating that the corresponding canonical variables are closely related. Moreover, it can be seen that the five groups of canonical variables have passed the hypothesis test of correlation significance. Considering the significant level of 0.05, two canonical correlation variables, (u_1, v_1) and (u_2, v_2), are retained to evaluate the relationship between the adjustment factors and accuracy indicators.

Table 6. Canonical correlation coefficients and the hypothesis test statistics.

Serial Number	1	2	3	4	5
Canonical correlation coefficients	0.99	0.94	0.92	0.74	0.57
Degree of Freedom	50	36	24	14	6
Calculated value of χ^2	105.84	58.48	34.26	13.47	4.87
Critical value of χ^2 (significance level is 0.05)	0.0000070	0.010	0.080	0.49	0.56

Table 7 shows the canonical structure between adjustment factors and canonical correlation variables. In the first canonical variables, the regional topographic factors, especially the elevation factor with a coefficient of -0.71 , show a strong negative correlation with u_1 . The three factors in the set of image TPs factors and the factor of overlap degree in the image set all have high coefficient values, whose coefficients are 0.52 , 0.48 , 0.50 , and 0.48 , respectively. Additionally, the situation of these five factors is similar italics in v_1 . This means that these five factors are the main factors in terms of adjustment factors, among which the topographic elevation factor and TPs factors are more important. The minimum in u_1 corresponds to the factor of image periods x_6 , which means that the role of image periods in the variation of accuracy is not very obvious.

Table 7. Canonical structure (correlation coefficients) for adjustment factors and canonical correlation variables.

Adjustment Factors X		u_1	u_2	v_1	v_2
The set of regional topographic factors	Average elevation x_1	-0.71	-0.35	-0.71	0.33
	Average slope x_2	-0.32	0.32	-0.31	-0.30
	Average roughness x_3	-0.26	0.40	-0.26	-0.37
The set of participating image factors	Images area x_4	0.11	0.70	0.11	-0.66
	Images number x_5	0.24	0.59	0.24	-0.55
	Images periods x_6	-0.06	0.35	-0.064	-0.33
	Images overlap degree x_7	0.48	0.50	0.47	-0.47
The set of image TPs factors	TPs number x_8	0.52	0.49	0.51	-0.46
	TPs density x_9	0.48	0.34	0.48	-0.33
	TPs nearest neighbor coefficient x_{10}	0.50	0.58	0.50	-0.55

Table 8 shows the canonical structure between accuracy indicators and canonical correlation variables. There is a strong relationship between Y -RMSE of accuracy indicators in object space and the first canonical vector v_1 , for which the correlation coefficient is 0.68 , followed by H -RMSE and X -RMSE, with coefficients of -0.45 and -0.39 , respectively. The correlation coefficients of s -RMSE and l -RMSE in image space are opposite for v_1 , as are the coefficients of X -RMSE and Y -RMSE in object space. That means the l -RMSE is the suppression variable in the accuracy indicators, and the value of the s -RMSE is small, but the value of the l -RMSE may be larger in the adjustment results. It is similar for X -RMSE and Y -RMSE in object space. This also indicates that there is a strong correlation in plane accuracy between image space and object space. The proportion of H -RMSE in v_1 and v_2 is relatively stable (-0.45 , -0.24). The degree of importance among the five accuracy indicators is not particularly obvious, while the proportion of l -RMSE in image space is slightly weak.

Table 8. Canonical structure (correlation coefficients) for accuracy indicators and canonical correlation variables.

Accuracy Indicators Y		v_1	v_2	u_1	u_2
Accuracy indicators in image space	s -RMSE y_1	-0.24	0.78	-0.24	-0.74
	l -RMSE y_2	0.16	0.14	0.16	-0.13
Accuracy indicators in object space	X -RMSE y_3	-0.39	0.83	-0.39	-0.79
	Y -RMSE y_4	0.68	0.066	0.67	-0.062
	H -RMSE y_5	-0.45	-0.24	-0.45	0.22

Furthermore, from the relationship between the accuracy indicators and u_1 , u_2 , there is a better prediction for Y -RMSE in object space in u_1 (0.67), while u_2 has a better prediction for X -RMSE in object space (-0.74) and s -RMSE in image space (-0.79). The prediction for

H -RMSE in u_1 and u_2 is middle ($-0.45, 0.22$), and the prediction for l -RMSE in image space is the weakest, with coefficients of only 0.16 and -0.13 .

4.4. Different Combinations of Regional Block Adjustments

As the set of image TPs factors and the set of participating image factors, especially the image overlap degree, have a high impact on accuracy, new TPs and image combinations in block adjustment are used to test the influence on accuracy in the three regions. Table 9 lists the accuracy statistics using different numbers of TPs in three regions. In the 08HZ region, H -RMSE has decreased from 2.66 m to 1.87 m with 4 multiples TPs, and the residuals in the s and l directions and the X - Y directions have all decreased. In the 07MS region, H -RMSE decreased from 2.78 m to 2.14 m with 2 multiple TPs but increased to 3.22 m with 4 multiple TPs. In the 01TJ region, H -RMSE decreased from 4.11 m to 3.46 m with 2 multiple TPs and 3.55 m with 4 multiple TPs, but there was little improvement in planar directions. The density of TPs in three regions is 0.21~0.85 points per km^2 , 0.38~1.50 points per km^2 , and 1.06~4.25 points per km^2 , respectively. The results indicate that more TPs will decrease the residuals both in elevation and planar directions, but more is not always better. In the 08HZ and 07MS regions with higher elevation fluctuation, the accuracy is best when the density of TPs is about 0.75~0.85 points per km^2 , while the accuracy would be better if the density of TPs is about 1.06~2.12 points per km^2 in the flatter 01TJ region.

Table 9. The accuracy with block adjustment using new TPs in three regions.

Region	Periods of Participated Images	TPs Number	Residuals in Image Space (Pixel)		Residuals in Object Space (Meter)		
			s -RMSE	l -RMSE	X -RMSE	Y -RMSE	H -RMSE
08HZ	5 (H1 H2 H3 H4 H5)	1 multiple	1.09	2.90	0.99	1.67	2.66
	5 (H1 H2 H3 H4 H5)	2 multiples	1.22	2.60	0.95	1.37	2.08
	5 (H1 H2 H3 H4 H5)	4 multiples	1.11	1.91	0.83	1.28	1.87
07MS	7 (M1M2M3M4M5M6M7)	1 multiple	4.12	2.24	2.83	0.91	2.78
	7 (M1M2M3M4M5M6M7)	2 multiples	4.28	2.04	2.961	0.84	2.14
	7 (M1M2M3M4M5M6M7)	4 multiples	4.76	1.89	3.262	0.37	3.22
01TJ	8 (T1T2T3T4T5T6T7T8)	1 multiple	1.37	3.83	0.70	2.60	4.11
	8 (T1T2T3T4T5T6T7T8)	2 multiples	1.82	3.48	1.04	2.61	3.46
	8 (T1T2T3T4T5T6T7T8)	4 multiples	1.76	3.51	1.00	2.62	3.55

Since the coverages of images in T1 and T2 are almost the same, T3, T4, T5, T6, and T7 also have similar coverages of images, respectively. Then, the images are selected to participate in the block adjustment. Table 10 lists the results of block adjustment with different combinations in the 01TJ region. Compared with the results in Table 5 in this region, the more images involved in the block adjustment under the same coverage condition, the better the accuracy has improved to some extent. For example, the combination of 2 periods (T1T2, T1T3, T1T4, T2T3, and T2T4) is obviously better than that of 1 single period T1, especially H -RMSE decreased from 5.88 m to 3.57 m, 4.25 m, 3.33 m, 1.36 m, and 2.18 m, respectively. Similarly, the combination of 5 periods (T1T2T3T4T5) is obviously better than that of 2 periods T1T4. The combination of (T1T4T7) is also improved compared to the combination of (T1T4). However, there is a decline in accuracy. That is, when the images in the T8 period are added in block adjustment, the residuals in both image space and object space become larger. The results are similar to those in Table 5. The H -RMSE in the combination of (T1T4T7T8) is 4.83 m, which is larger than 3.17 in the combination of (T1T4T7). The combinations of T1T3, T1T4, T2T3, and T2T4 have almost the same coverage area, but the residuals of block adjustment are different, especially for the elevation residuals ranging from 1.36 m to 4.25 m.

Table 10. The accuracy of block adjustment with selected images in the 01TJ region.

Periods of Participated Images	Number of Images Pairs	Residuals in Image Space (Pixel)		Residuals in Object Space (Meter)		
		<i>s</i> -RMSE	<i>l</i> -RMSE	<i>X</i> -RMSE	<i>Y</i> -RMSE	<i>H</i> -RMSE
4 (T1T4T7T8)	11	2.07	5.39	0.77	3.77	4.83
3 (T1T4T7)	8	1.94	4.29	0.82	3.40	3.17
2 (T2T4)	6	1.74	2.99	1.94	6.29	2.18
2 (T2T3)	6	3.75	5.03	1.92	4.10	1.36
2 (T1T4)	6	2.37	4.81	0.93	3.95	3.33
2 (T1T3)	6	1.71	3.12	0.79	2.32	4.25
1 (T1)	3	1.74	2.99	1.15	1.41	5.88

5. Discussion

5.1. Influence Characteristics of Adjustment Factors on the Accuracy

The influence of three sets of adjustment factors on accuracy is different. For the accuracy in image space, the factors that affect the accuracy are successively the set of image TPs factors, the set of participating image factors, and the set of regional topographic factors according to their degree of importance. While the factors are successively the set of image TPs factors, the set of regional topographic factors, and the set of participating image factors according to the degree of importance for accuracy in object space. However, there are different problems, such as different matching errors, different jitter states, and others, in different regions, which also need to be considered in the adjustment and evaluation.

The set of image TP factors plays the most important role in the accuracy evaluation, both in image space and object space. Therefore, improving the quality of TPs can effectively improve accuracy not only in image space but also in object space. The difference between the three TPs factors is not obvious since they have related mathematical definitions, and the quantity of TPs is a very basic and important factor based on the results in Figure 3. However, the nearest neighbor coefficient of TPs is more closely related to accuracy than the number and density of TPs. This also means that a better distribution of TPs in the stage of image matching is actually more critical to accuracy when enough TPs are generated using a certain method. However, the results in Section 4.4 show that the more TPs, the better. In regions with large elevation fluctuations, more TPs can effectively improve positioning accuracy. Further, too many TPs will also cause a decline in accuracy.

The set of regional topographic factors has a deep influence on both plane and elevation accuracy. From the mathematical definition of the three topographic factors, it can be seen that both slope and roughness are directly related to elevation, and both are variations in elevation in the region. Moreover, the average elevation factor has the highest canonical correlation coefficient (-0.71), so the overall influence of the elevation factor is more significant than the other two topographic factors. However, the influence of three topographic factors on accuracy in the three regions is different. The correlation coefficients between topographic factors and the five accuracy indicators calculated independently for each region are listed in Table 11. Not exactly the same as Figure 4, the results of the individual analysis show that the influence of three topographic factors on the five accuracy indicators is more balanced in the 08HZ region, while the factors have more influence on the *s* and *Y* directions in the 07MS region. In the 01TJ region, the influence of topographic factors in all directions is relatively balanced, and the elevation factor among the three factors is obviously more important in this region. From the elevation distribution of the three regions, plain and mountain coexist in the 08HZ and 07MS regions, both of which have higher elevations, while 01TJ is relatively flat and the overall elevation is low. That means the difference in topographic factors will also cause a difference in adjustment accuracy, even with the same adjustment method and parameter selection. Further analysis should be needed with more experiments in different terrain regions.

The set of participating image factors reflects image quality in the block adjustment. Even with the same coverage, the different image combinations will lead to differences in accuracy, such as the combinations T1T3, T1T4, T2T3, and T2T4 in Table 10. Their

accuracy performance in the plane and elevation directions is different, which may need to be considered in combination with topographic factors in the future. Image overlap is the most important factor in this group and is strongly related to the number of TPs, while the subsequent important factors are the number of images. The decrease in image overlap would lead to a decrease in accuracy to some extent, even if more images participated in the adjustment. For example, the residuals increase after the images of T8 are added in the block adjustment, partly due to the low overlap of T8 with other images in the 01TJ region.

On the other hand, the coverage area and periods of the participating images are not significantly affected by accuracy, especially the image periods. Figure 5 shows the variation of RMSE values in image space and object space with periods of image pairs participating in three study regions. It can be seen that the overall change is modest with the periods of image pairs. Therefore, it is crucial to consider the degree of overlap between images in the selection of participating images in order to improve accuracy.

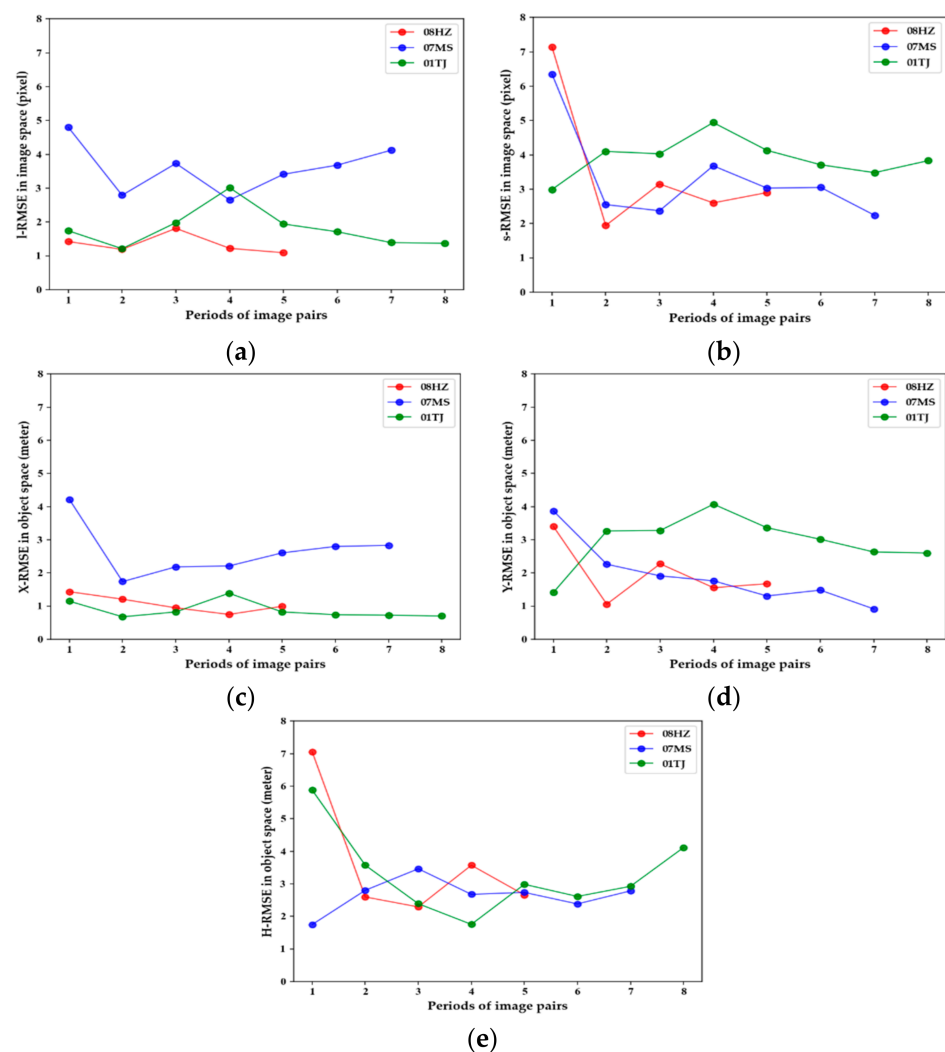


Figure 5. Variation of RMSE values in object space and image space with periods of image pairs participating in three study regions. (a) Variation of *l*-RMSE values in image space; (b) Variation of *s*-RMSE values in image space; (c) Variation of *X*-RMSE values in object space, (d) Variation of *Y*-RMSE values in object space; (e) Variation of *H*-RMSE values in object space.

The influence of the image number factor on accuracy tends to be stable when the number of images exceeds a certain number (15) in the regional block adjustment for GF-7 stereo imagery. Figure 6 shows the variation of RMSE values with the number of image pairs participating in all study areas. The figures indicate that the relationship between

the accuracy indicators and the number of image pairs is not obvious both in the image and object space when the number of image pairs participating in the adjustment is small (less than 15). However, when the number of image pairs involved in adjustment tends to increase, the overall accuracy improves and gradually becomes stable.

Table 11. Correlation coefficients between the accuracy indicators and topographic factors calculated independently for each region.

Region	Topographic Factors	Correlation Coefficients				
		s-RMSE	l-RMSE	X-RMSE	Y-RMSE	H-RMSE
08HZ	Average elevation	0.35	0.52	0.69	0.44	0.59
	Average slope	0.35	0.44	0.61	0.37	0.53
	Average roughness	0.34	0.44	0.62	0.36	0.53
07MS	Average elevation	0.13	−0.47	0.02	−0.77	0.09
	Average slope	0.16	−0.49	0.01	−0.78	0.16
	Average roughness	0.14	−0.51	−0.01	−0.79	0.17
01TJ	Average elevation	0.74	0.64	0.39	0.72	−0.77
	Average slope	0.48	0.28	0.51	0.26	−0.14
	Average roughness	0.47	0.27	0.51	0.26	−0.14

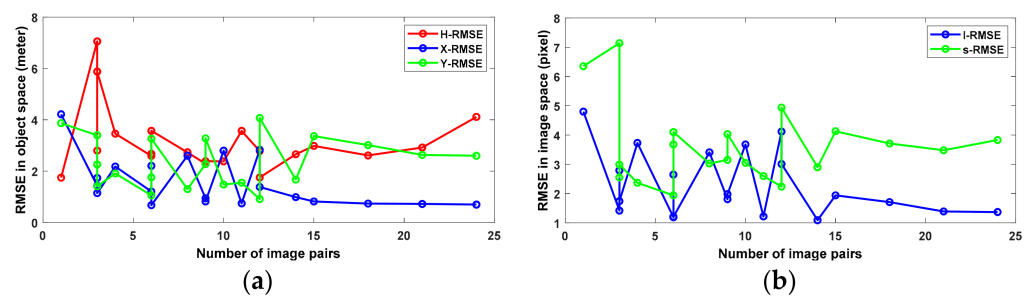


Figure 6. Variation of RMSE values with a number of image pairs participating for all study areas. (a) Variation of RMSE values in object space; (b) Variation of RMSE values in image space.

5.2. Influence of Non-Adjustment Factors on Accuracy

There is a correlation among the accuracy variables from the results of correlation coefficients and the canonical correlation analysis, especially between the *s* direction in image space and the *X* direction in object space, and so the *l* direction and *Y* direction. Moreover, their variations are very similar, which means there is a strong correlation in plane accuracy between image space and object space. However, the elevation accuracy in the *H* direction is relatively independent and more balanced under the influence of three sets of adjustment factors.

It should be noted that these accuracy indicators are almost equally important in the set of accuracy variables, which can represent the variation level of accuracy, but the degree of influence by the three sets of factors is different. Moreover, the correlation coefficients are sensitive to outliers and mainly describe the linear relationship between two variables. The non-linear relationship between the adjustment factors and accuracy indicators needs to be considered in the future. There are also accuracy indicators that cannot be determined by the ten factors, although the accuracy is closely related to the three sets of ten factors. As for the accuracy in the *l* direction in image space, the existing ten factors have not been well expressed and predicted for it. This also indicates that there are other inherent factors, not within the range of these ten factors, that should be related to the physical characteristics of *l*, such as the CCD camera. The correction of internal parameters for the GF-7 stereo camera may be more critical than the block adjustment, and introducing the internal parameters as unknowns into the block adjustment is also a solution to improve the accuracy, especially in image space.

6. Conclusions

This paper proposes a correlation analysis between the accuracy indicators and three sets of ten adjustment factors, including topographic factors, participating image factors, and TPs factors, to quantify the influence of adjustment factors on accuracy and then evaluate the accuracy of the regional block adjustment without GCPs for GF-7 stereo imagery. The results show that block adjustment without GCPs can improve direct positioning accuracy; at the same time, the three sets of adjustment factors have different effects on accuracy. The following conclusions are obtained:

- (1) The positioning accuracy does not deteriorate with time for GF-7 satellite imagery. The RFM-based regional block adjustment without GCPs can improve the direct positioning accuracy for GF-7 stereo imagery, but the improvement is affected by the factors of regional topography, the participating images, and the TPs involved in the adjustment.
- (2) The set of TP factors is the most influential factor set among the three sets of ten adjustment factors. Therefore, improving the quality of TPs, especially their more uniform distribution, is the key to improving the accuracy of regional block adjustment.
- (3) Topographic factors also play an important role in the adjustment of Gaofen-7 stereo imagery without GCPs. The influence of topographic factors on accuracy is different in different regions. Further, the influence of the elevation factor, with the highest canonical correlation coefficient (-0.71), is more significant than the other two factors.
- (4) The influence of image overlap on accuracy is more critical than the image coverage area, number, and time periods for the selection of images participating in adjustment. At the same time, the influence of image number on accuracy does not change much when the number of images exceeds a certain number (15 pairs) for GF-7 images. In other words, under the condition that the overlap of images is satisfied, this is of great referential significance for the partition processing of large-area block adjustment for GF-7 stereo imagery.
- (5) The five accuracy indicators used in this paper can reflect the level of adjustment accuracy, but the influence of three sets of factors is different. The ten adjustment factors have less influence on the accuracy of image space, especially the s direction in image space, which is related to the physical characteristics of the image from the camera. This can be inferred from the fact that its improvement requires the internal inspection and correction of the images, or from the unknown reflected in the regional block adjustment.

Author Contributions: X.T. and X.Z. developed the main idea of this study and performed the data processing and analysis. W.H. and J.D. gave support to the DEM generation and accuracy analysis and the discussion of the results. The detailed information is as follows: Data curation, X.Z. and W.H.; formal analysis, X.Z. and W.H.; methodology, X.Z.; project administration, X.Z. and X.T.; supervision, J.D. All authors have read and agreed to the published version of the manuscript.

Funding: This research was supported by the High-Resolution Remote Sensing, Surveying, and Mapping Application Demonstration System (Phase II) (NO. 42-Y30B04-9001-19/21) and the National Natural Science Foundation of China (Grant No. 41201361).

Data Availability Statement: GF-7 imagery can be inquired through the website, Natural Resource Satellite Remote Sensing Cloud Service Platform (<http://sasclouds.com/english/home>). Illustrations in this paper were subject to no copyright restrictions.

Acknowledgments: We thank the editors for their editorial help as well as academic suggestions from the anonymous reviewers.

Conflicts of Interest: The authors declare no conflict of interest.

Appendix A

Table A1. The specific values of adjustment factors from the regional block adjustments results.

Experimental Serial Number	The Set of Regional Topographic Factors			The Set of Participating Image Factors			The Set of Image TPs Factors			
	Average Elevation	Average Slope	Average Roughness	Images Area	Images Number	Images Periods	Degree of Images Overlap	TPs Number	TPs Density	TPs Nearest Neighbor Coefficient
(1)	69.55	7.48	11.28	59,601.00	14	5	47.61%	1263	0.212	0.60
(2)	92.51	9.44	14.07	4277.03	11	4	58.86%	1072	0.251	0.58
(3)	99.08	9.75	14.54	3813.39	9	3	46.22%	809	0.212	0.59
(4)	112.20	10.74	16.06	2221.78	6	2	66.84%	509	0.229	0.61
(5)	121.47	11.13	16.60	1645.40	3	1	9.22%	246	0.15	0.65
(6)	173.07	4.77	6.56	2983.67	12	7	68.36%	1118	0.375	0.34
(7)	171.45	4.75	6.52	2956.36	10	6	61.51%	1111	0.376	0.35
(8)	156.97	4.57	6.28	2711.86	8	5	37.67%	1065	0.393	0.35
(9)	102.21	4.01	5.52	1846.39	6	4	45.85%	726	0.393	0.38
(10)	106.00	4.16	5.72	1671.29	4	3	38.37%	572	0.342	0.37
(11)	88.28	3.82	5.26	1466.91	3	2	27.20%	265	0.181	0.47
(12)	84.71	3.82	5.23	701.92	1	1	0	152	0.217	0.49
(13)	10.02	2.99	4.89	5666.49	24	8	70.77%	6023	1.063	0.57
(14)	10.24	3.26	5.34	4057.01	21	7	92.93%	5839	1.439	0.59
(15)	10.26	3.29	5.38	3912.78	18	6	81.43%	5638	1.441	0.59
(16)	10.42	3.46	5.66	3267.32	15	5	84.66%	5233	1.602	0.61
(17)	10.50	3.55	5.81	3022.01	12	4	90.57%	5036	1.666	0.60
(18)	10.50	3.55	5.81	3022.01	9	3	61.95%	5036	1.666	0.60
(19)	10.17	3.53	5.79	1733.50	6	2	93.91%	2971	1.714	0.55
(20)	10.11	3.52	5.77	1667.33	3	1	10.68%	2965	1.778	0.56

Table A2. The specific values of accuracy indicators from the regional block adjustments results.

Experimental Serial Number	Accuracy Indicators				
	<i>l</i> -RMSE (Pixel)	<i>s</i> -RMSE (Pixel)	<i>X</i> -RMSE (m)	<i>Y</i> -RMSE (m)	<i>H</i> -RMSE (m)
(1)	1.09	2.9	0.99	1.672	2.658
(2)	1.22	2.6	0.746	1.552	3.57
(3)	1.81	3.15	0.945	2.273	2.289
(4)	1.19	1.94	1.205	1.055	2.595
(5)	1.42	7.14	1.432	3.400	7.053
(6)	4.12	2.24	2.830	0.913	2.782
(7)	3.68	3.05	2.797	1.479	2.381
(8)	3.41	3.03	2.603	1.303	2.735
(9)	2.65	3.68	2.208	1.759	2.675
(10)	3.73	2.37	2.181	1.909	3.461
(11)	2.79	2.55	1.736	2.260	2.8
(12)	4.80	6.35	4.216	3.869	1.748
(13)	1.37	3.83	0.698	2.598	4.113
(14)	1.39	3.48	0.723	2.631	2.922
(15)	1.71	3.71	0.738	3.013	2.611
(16)	1.94	4.13	0.82	3.363	2.983
(17)	3.01	4.94	1.385	4.072	1.753
(18)	1.98	4.03	0.821	3.279	2.387
(19)	1.21	4.1	0.674	3.265	3.571
(20)	1.74	2.99	1.145	1.409	5.879

Table A3. The detailed accuracy of direct stereo positioning with the original RPC for each single image pair in 08HZ region.

Period of Images	Acquisition Time of Images	Central Latitude and Longitude of Images	Accuracy of Direct Stereo Positioning			Accuracy of Block Adjustment in Each Single Time Period		
			<i>X</i> -RMSE (m)	<i>Y</i> -RMSE (m)	<i>H</i> -RMSE (m)	<i>X</i> -RMSE (m)	<i>Y</i> -RMSE (m)	<i>H</i> -RMSE (m)
H1	2020-06-26 3 pairs (6 scenes)	E119.5_N30.7	3.750	2.894	6.621	1.432	3.400	7.053
		E119.6_N30.9	3.939	2.736	7.950			
		E119.6_N31.1	4.069	2.838	4.414			
H2	2021-11-24 3 pairs (6 scenes)	E119.6_N30.7	2.664	2.897	2.248	0.984	3.343	2.319
		E119.6_N30.9	1.778	3.063	1.636			
		E119.7_N31.1	2.583	2.250	1.372			

Table A3. *Cont.*

Period of Images	Acquisition Time of Images	Central Latitude and Longitude of Images	Accuracy of Direct Stereo Positioning			Accuracy of Block Adjustment in Each Single Time Period		
			X-RMSE (m)	Y-RMSE (m)	H-RMSE (m)	X-RMSE (m)	Y-RMSE (m)	H-RMSE (m)
H3	2022-01-03 3 pairs (6 scenes)	E119.9_N30.7	2.425	5.891	1.584	1.291	4.991	1.465
		E119.9_N30.9	2.531	5.291	1.433			
		E119.9_N31.1	3.075	5.122	1.232			
H4	2020-09-03 2 pairs (4 scenes)	E120.0_N30.7	1.864	2.361	2.130	1.414	2.259	2.083
		E120.0_N30.9	2.160	2.267	1.427			
H5	2020-05-03 3 pairs (6 scenes)	E120.2_N30.7	1.404	0.774	2.694	1.653	0.953	2.819
		E120.1_N30.5	1.481	0.662	2.385			
		E120.2_N30.9	1.385	0.691	3.337			

Table A4. The detailed accuracy of direct stereo positioning with the original RPC for each single image pair in 07MS region.

Period of Images	Acquisition Time	Central Latitude and Longitude of Images	Accuracy of Direct Stereo Positioning			Accuracy of Block Adjustment in Each Single Time Period		
			X-RMSE (m)	Y-RMSE (m)	H-RMSE (m)	X-RMSE (m)	Y-RMSE (m)	H-RMSE (m)
M1	2020-04-23 1 pair (2 scenes)	E4.9_N43.7	2.321	4.395	0.817	2.321	4.395	0.817
M2	2020-07-01 2 pairs (4 scenes)	E5.1_N43.7	1.689	3.708	9.677	0.786	5.049	5.970
		E5.0_N43.5	2.378	4.763	7.339			
M3	2020-05-18 1 pair (2 scenes)	E5.2_N43.7	1.153	0.538	2.645	1.153	0.538	2.645
M4	2020-09-03 2 pairs (4 scenes)	E5.2_N43.7	3.637	5.219	4.377	2.432	5.377	3.0169
		E5.1_N43.5	2.415	5.097	2.028			
M5	2021-08-28 2 pairs (4 scenes)	E5.3_N43.5	3.813	1.336	2.535	3.034	1.938	1.988
		E5.4_N43.7	4.549	2.570	1.003			
M6	2021-06-30 2 pairs (4 scenes)	E5.4_N43.7	3.678	0.903	3.974	3.827	1.354	4.972
		E5.4_N43.5	2.980	1.612	5.208			
M7	2021-05-02 2 pairs (4 scenes)	E5.4_N43.5	2.463	5.641	3.139	3.248	5.404	2.733
		E5.5_N43.7	3.085	4.538	1.224			

Table A5. The detailed accuracy of direct stereo positioning with the original RPC for each single image pair in 01TJ region.

Period of Images	Acquisition Time	Central Latitude and Longitude of Images	Accuracy of Direct Stereo Positioning			Accuracy of Block Adjustment at Each Single Time Period		
			X-RMSE (m)	Y-RMSE (m)	H-RMSE (m)	X-RMSE (m)	Y-RMSE (m)	H-RMSE (m)
T1	2020-12-24 3 pairs (6 scenes)	E116.9_N39.0	0.484	1.679	3.706	1.341	1.354	5.803
		E117.0_N39.2	0.676	1.836	6.259			
		E117.0_N39.4	0.912	0.891	3.429			
T2	2021-06-19 3 pairs (6 scenes)	E116.9_N39.0	0.661	5.407	0.990	0.979	5.584	2.209
		E117.2_N39.4	0.714	5.078	3.413			
		E116.9_N39.2	0.835	5.729	2.525			
T3	2021-09-21 3 pairs (6 scenes)	E117.1_N39.0	7.310	2.844	6.836	4.666	2.453	4.457
		E117.1_N39.2	6.711	3.154	5.504			
		E117.2_N39.4	6.121	2.891	3.971			
T4	2022-02-10 3 pairs (6 scenes)	E117.1_N39.0	3.898	6.975	0.746	2.750	6.630	1.521
		E117.1_N39.2	3.914	7.308	1.226			
		E117.2_N39.4	3.101	6.059	1.268			
T5	2020-12-14 3 pairs (6 scenes)	E117.1_N39.0	0.833	1.838	4.550	1.679	2.424	4.684
		E117.2_N39.4	1.399	2.051	4.913			
		E117.2_N39.2	0.927	2.236	4.190			
T6	2020-05-22 3 pairs (6 scenes)	E117.2_N39.0	3.043	0.839	2.011	1.100	0.971	2.185
		E117.3_N39.2	3.224	1.013	1.568			
		E117.3_N39.4	3.333	1.641	2.481			
T7	2020-11-05 3 pairs (6 scenes)	E117.3_N39.2	1.383	1.511	4.153	2.869	1.087	6.632
		E117.4_N39.4	1.555	1.050	6.901			
		E117.3_N39.0	1.450	1.167	4.038			
T8	2021-05-01 3 pairs (6 scenes)	E117.5_N39.0	1.186	5.809	2.681	1.031	6.137	2.687
		E117.4_N38.8	0.938	6.088	1.894			
		E117.6_N39.2	1.095	7.128	2.093			

References

1. Cao, H.; Tao, P.; Liu, Y.; Li, H. Nonlinear Systematic Distortions Compensation in Satellite Images Based on an Equivalent Geometric Sensor Model Recovered From RPCs. *IEEE J. Sel. Top. Appl. Earth Obs. Remote Sens.* **2021**, *14*, 12088–12102. [[CrossRef](#)]
2. Radhadevi, P.V.; Müller, R.; d'Angelo, P.; Reinartz, P. In-flight Geometric Calibration and Orientation of ALOS/PRISM Imagery with a Generic Sensor Model. *Photogramm. Eng. Remote Sens.* **2011**, *77*, 531–538. [[CrossRef](#)]
3. Takaku, J.; Tadono, T. RPC generations on ALOS PRISM and AVNIR-2. In Proceedings of the IEEE International Geoscience and Remote Sensing Symposium (IGARSS), Vancouver, BC, Canada, 24–29 July 2011.
4. Tang, X.; Zhou, P.; Zhang, G.; Wang, X.; Pan, H. Geometric Accuracy Analysis Model of the Ziyuan-3 Satellite without GCPs. *Photogramm. Eng. Remote Sens.* **2015**, *81*, 927–934. [[CrossRef](#)]
5. Toutin, T. Geometric processing of remote sensing images: Models, algorithms and methods. *Int. J. Remote Sens.* **2010**, *25*, 1893–1924. [[CrossRef](#)]
6. Valadan Zoej, M.J.; Mokhtarzade, M.; Mansourian, A.; Ebadi, H.; Sadeghian, S. Rational function optimization using genetic algorithms. *Int. J. Appl. Earth Obs. Geoinf.* **2007**, *9*, 403–413. [[CrossRef](#)]
7. Yang, B.; Wang, M.; Xu, W.; Li, D.; Gong, J.; Pi, Y. Large-scale block adjustment without use of ground control points based on the compensation of geometric calibration for ZY-3 images. *ISPRS J. Photogramm. Remote Sens.* **2017**, *134*, 1–14. [[CrossRef](#)]
8. Zhang, Y.; Lu, Y.; Wang, L.; Huang, X. A New Approach on Optimization of the Rational Function Model of High-Resolution Satellite Imagery. *IEEE Trans. Geosci. Remote Sens.* **2012**, *50*, 2758–2764. [[CrossRef](#)]
9. Gong, J.; Wang, M.; Yang, B. High-precision Geometric Processing Theory and Method of High-Resolution Optical Remote Sensing Satellite Imagery without GCP. *Acta Geod. Cartograph. Sin.* **2017**, *46*, 1255–1261.
10. Zhang, Y.; Wan, Y.; Shi, W.; Zhang, Z.; Li, Y.; Ji, S.; Gu, H.; Li, L. Technical Framework and Preliminary Practices of Photogrammetric Remote Sensing Intelligent Processing of Multi-Source Satellite Images. *Acta Geod. Cartograph. Sin.* **2021**, *50*, 1068–1083.
11. Zhang, L.; Liu, Y.; Sun, Y.; Lan, C.; Ai, H.; Fan, Z. A Review of Developments in the Theory and Technology of Three-Dimensional Reconstruction in Digital Aerial Photogrammetry. *Acta Geod. Cartograph. Sin.* **2022**, *51*, 1437–1457.
12. Yang, B.; Wang, M.; Pi, Y. Block Adjustment without GCPs for Large-scale Regions only Based on the Virtual Control Points. *Acta Geod. Cartograph. Sin.* **2017**, *46*, 874–881.
13. Zheng, M.; Zhang, Y.; Zhou, S.; Zhu, J.; Xiong, X. Bundle block adjustment of large-scale remote sensing data with Block-based Sparse Matrix Compression combined with Preconditioned Conjugate Gradient. *Comput. Geosci.* **2016**, *92*, 70–78. [[CrossRef](#)]
14. Aurélie, B.; Marc, B.; Patrick, G.; Alain, O.; Véronique, R.; Alain, B. SPOT 5 HRS geometric performances: Using block adjustment as a key issue to improve quality of DEM generation. *ISPRS J. Photogramm. Remote Sens.* **2006**, *60*, 134–146.
15. Liu, B.; Jia, M.; Di, K.; Oberst, J.; Xu, B.; Wan, W. Geopositioning precision analysis of multiple image triangulation using LROC NAC lunar images. *Planet. Space Sci.* **2018**, *162*, 20–30. [[CrossRef](#)]
16. Tao, P.; Xi, K.; Niu, Z.; Chen, Q.; Liao, Y.; Liu, Y.; Liu, K.; Zhang, Z. Optimal selection from extremely redundant satellite images for efficient large-scale mapping. *ISPRS J. Photogramm. Remote Sens.* **2022**, *194*, 21–38. [[CrossRef](#)]
17. Wang, C.; Sun, Z.; Liang, Z.; Zhang, J. Refined Identification of Winter Wheat Area Based on GF-7 Satellite Remote Sensing. *J. Anhui Agric. Sci.* **2021**, *49*, 244–247, 252.
18. Li, G.; Tang, X. Accuracy evaluation of large lake water level measurement based on GF-7 laser altimetry data. *Natl. Remote Sens. Bull.* **2022**, *26*, 138–147.
19. Luo, H.; He, B.A.; Guo, R.; Wang, W.; Kuai, X.; Xia, B.; Wan, Y.; Ma, D.; Xie, L. Urban Building Extraction and Modeling Using GF-7 DLC and MUX Images. *Remote Sens.* **2021**, *13*, 3414. [[CrossRef](#)]
20. Zhang, C.; Cui, Y.; Zhu, Z.; Jiang, S.; Jiang, W. Building Height Extraction from GF-7 Satellite Images Based on Roof Contour Constrained Stereo Matching. *Remote Sens.* **2022**, *15*, 7. [[CrossRef](#)]
21. Wang, J.; Hu, X.; Meng, Q.; Zhang, L.; Wang, C.; Liu, X.; Zhao, M. Developing a Method to Extract Building 3D Information from GF-7 Data. *Remote Sens.* **2021**, *13*, 4532. [[CrossRef](#)]
22. Chen, C.; Ding, J.; Wang, S.; Liu, J. High-precision control technology and on-orbit verification of GF-7 satellite. *Chin. Space Sci. Technol.* **2020**, *40*, 34–41.
23. Zhou, P.; Tang, X. Geometric Accuracy Verification of GF-7 Satellite Stereo Imagery Without GCPs. *IEEE Geosci. Remote Sens. Lett.* **2022**, *19*, 1–5. [[CrossRef](#)]
24. Xie, Y.; Gui, M. DEM Production Based on GF-7 Stereo Pairs and The Accuracy Verification. *Surv. Mapp.* **2021**, *44*, 163–165.
25. Hu, L.; Tang, X.; Zhang, Z.; Li, G.; Chen, J.; Tian, H.; Zhang, S.; Qiao, J.; Li, X. Accuracy Optimization and Assessment of GF-7 Satellite Multi-source Remote Sensing Data. *Infrared Laser Eng.* **2022**, *51*, 1–9.
26. Chen, J.; Tang, X.; Xue, Y.; Li, G.; Zhou, X.; Hu, L.; Zhang, S. Registration and Combined Adjustment for the Laser Altimetry Data and High-Resolution Optical Stereo Images of the GF-7 Satellite. *Remote Sens.* **2022**, *14*, 1666. [[CrossRef](#)]
27. Pi, Y.; Yang, B.; Li, X.; Wang, M. Robust Correction of Relative Geometric Errors Among GaoFen-7 Regional Stereo Images Based on Posterior Compensation. *IEEE J. Sel. Top. Appl. Earth Obs. Remote Sens.* **2022**, *15*, 3224–3234. [[CrossRef](#)]
28. Zhu, X.; Tang, X.; Zhang, G.; Liu, B.; Hu, W. Accuracy Comparison and Assessment of DSM Derived from GFDM Satellite and GF-7 Satellite Imagery. *Remote Sens.* **2021**, *13*, 4791. [[CrossRef](#)]
29. Song, J.; Fan, D.; Ji, S.; Li, D.; Chu, G. Laser Spot Centroid Extraction of GF-7 Footprint Images. *J. Geomat. Sci. Technol.* **2021**, *38*, 507–513.

30. Luo, H.; He, B.; Guo, R.; Wang, W.; Kuai, X.; Xia, B. GF-7 image quality assessment and interpretability analysis. *Eng. Surv. Mapp.* **2022**, *31*, 1–7.
31. Tang, X.; Xie, J.; Liu, R.; Huang, G.; Zhao, C.; Zhen, Y.; Tang, H.; Dou, X. Overview of the GF-7 Laser Altimeter System Mission. *Earth Space Sci.* **2020**, *7*, 1. [[CrossRef](#)]
32. Si, S.; Sun, X. *Mathematical Modeling*; National Defense Industry Press: Beijing, China, 2014.
33. Tachikawa, T.; Hato, M.; Kaku, M. Characteristics of ASTER GDEM version 2. In Proceedings of the IEEE International Geoscience and Remote Sensing Symposium (IGARSS), Vancouver, BC, Canada, 24–29 July 2011.

Disclaimer/Publisher’s Note: The statements, opinions and data contained in all publications are solely those of the individual author(s) and contributor(s) and not of MDPI and/or the editor(s). MDPI and/or the editor(s) disclaim responsibility for any injury to people or property resulting from any ideas, methods, instructions or products referred to in the content.